

# Can active hydrodynamic fluctuations affect barrier crossing during enzymatic catalysis?

Ashwani Kr. Tripathi,<sup>1</sup> Tamoghna Das,<sup>1</sup> Govind Paneru,<sup>1</sup> Hyuk Kyu Pak,<sup>1,2,\*</sup> and Tsvi Tlusty<sup>1,2,3,†</sup>

<sup>1</sup>Center for Soft and Living Matter, Institute for Basic Science (IBS), Ulsan, 44919, Republic of Korea

<sup>2</sup>Department of Physics, Ulsan National Institute of Science and Technology, Ulsan, 44919, Republic of Korea

<sup>3</sup>Department of Chemistry, Ulsan National Institute of Science and Technology, Ulsan, 44919, Republic of Korea

(Dated: May 7, 2021)

The cellular milieu is teeming with biochemical nano-machines whose activity is a strong source of correlated non-thermal fluctuations termed “active noise”. Essential elements of this circuitry are enzymes, catalysts that speed up the rate of metabolic reactions by orders of magnitude, thereby making life possible. Here, we examine the possibility that active noise in the cell, or in vitro, affects enzymatic catalytic rate by accelerating or decelerating the crossing of energy barriers during reaction. Considering hydrodynamic perturbations induced by biochemical activity as a source of active noise, we attempt to evaluate their plausible impact on the enzymatic cycle using a combination of analytic and numerical methods. Our estimate shows that the fast component of the active noise spectrum may enhance the rate of enzymes, by up to 50%, while reactions remain practically unaffected by the slow noise spectrum and are mostly governed by thermal fluctuations. Revisiting the physics of barrier crossing under the influence of active hydrodynamic fluctuations suggests that the biochemical activity of macromolecules such as enzymes is coupled to active noise, with potential impact on metabolic networks in living and artificial systems alike.

## INTRODUCTION

The idea that enzymes achieve their phenomenal catalytic capacity by stabilizing an activated transition state was introduced by Haldane [1] and developed by Pauling [2] who lucidly stated this postulate [3]: “. . . that the enzyme has configuration complementary to the activated complex, and accordingly has the strongest power of attraction for the activated complex, means that the activation energy for the reaction is less in the presence of the enzyme than in its absence, and accordingly that the reaction would be speeded up by the enzyme.” Electrostatic effects, chiefly the formation of a preorganized polar network, were recognized as pivotal in stabilizing the transition state [4, 5]. In this extremely fruitful view of enzymatic catalysis, the activated complex is jolted past the transition state’s energy barrier by thermal agitation [6–8]. The cell, however, is bustling with activity that generates significant *athermal* agitation [9–13], provoking the main question asked in this paper: how may athermal active noise affect enzymatic catalysis?

During their catalytic cycle, many enzymes undergo conformational changes, for example to enable substrate binding and product release [14–25]. Such internal motions and rearrangements are part of essential mechanisms, particularly induced fit [26], conformational selection [27, 28] and allostery [29–33]. The coexistence of multiple conformational states [34] may assist evolution to explore new functions [35]. Motor proteins operate by converting chemical energy into conformational changes and motion [36–38], and recent studies suggest that similar coupling underlies the boosted diffusion observed in active enzymes [39–42]. Linkage between intrinsic motion and catalysis was reported in adenylate kinase (ADK) [43–47], dihydrofolate reductase (DHFR) [48–54], and other enzymes [51, 55, 56]—though the existence,

extent and physical nature of this linkage remain open questions [20, 21, 57]. All this invokes a notion of enzymes as stochastic molecular machines whose chemical performance and evolution are linked to their internal mechanics [51, 58–64].

For their nanometric size, these machines are subject to violent, thermal and athermal, agitation by the fluctuating environment: Thermal white noise originates from memoryless equilibrium fluctuations. Athermal *colored* noise is generated by a variety of temporally-correlated active sources, such as molecular motors and cytoskeleton rearrangement [9, 11, 13, 65–67], and the dynamics of other cellular machinery, including enzymes [39–42]. This work lays out a simple model in order to investigate how these thermal and athermal fluctuations, in vivo or in vitro, might affect the catalytic reaction rate. From a coarse-grained perspective, we treat enzymes as stochastic force dipoles [64, 68–71], each made of a pair of masses joined by a spring. The relative motion of the masses represent conformational changes of the enzyme during the catalytic cycle.

The framework developed here extends transition-rate theory [72–76] to account for the impact of correlated noise induced by hydrodynamic fluctuations. In principle, this method can be applied to other biological processes, such as unzipping of DNA and RNA hairpins [77–81] or generally, to any other physical process that can be cast as a two-state system with noisy memory. Using this model, we computed the reaction rate, relative to a purely thermally-fluctuating enzyme, as a function of the active noise strength and its correlation timescale. Within a biologically relevant parameter range typical to enzymes, we find two potential effects of active noise: Strong active noise with long correlation time (relative to the turnover rate) seems to hinder enzymatic activity, and the reaction slows down compared to a thermally-activated enzyme. However, active fluctuations of any strength with short to intermediate correlation times enhance the catalytic rate. Under the combined influence of thermal and active noise, in a biologically relevant regime, we find a potential increase of

\* hyuk.k.pak@gmail.com

† tsvitlusty@gmail.com

10–50% in the turnover rate for enzymes.

We start by deriving the active noise induced by hydrodynamic fluctuations, and then model the impact of the noise on the catalytic cycle. Next, we numerically estimate the potential effect of the noise strength and correlation time on a reaction in general. Finally, we present our main results on the variation of reaction rate in the presence of active noise and illustrate it with specific examples of enzymes. We discuss the implications of these findings and conclude with remarks about the general applicability and possible improvements of our study.

## MODEL

**Active noise realisation of hydrodynamic fluctuations.** An enzyme in a cellular environment continually experiences correlated stochastic forces, as a collective effect of diverse flow-generating mechanisms, which we model as sources of athermal active noise. To estimate these stochastic forces, we approximate the active noise sources as an ensemble of force dipoles. This is a valid long-range approximation as force dipoles induce the leading term in the far-field expansion of momentum-conserving hydrodynamic perturbations [82, 83]. Each force dipole is represented as two equal masses connected by a spring of rest length  $\ell$ . The cellular background is treated as a random ensemble of average concentration  $c_0$  of such force dipoles whose moments  $\{\mathbf{m}_i\}$  are randomly distributed at positions  $\{\mathbf{R}_i\}$  with randomly isotropic orientations  $\{\mathbf{e}_i\}$ .

As the typical inertial timescale ( $\sim 1$  ps) is much shorter than the characteristic timescale of an enzyme, ( $> 1$   $\mu$ s), the background flow is overdamped. It is therefore convenient to treat this linear Stokesian flow in terms of its Green function, the mobility tensor  $\mathcal{G}$ . A dipole  $\mathbf{m}$  made of a pair of opposing point forces will therefore generate a flow field  $\mathbf{v}(\mathbf{r})$  proportional to the gradient of the Green function,  $\mathbf{v}(\mathbf{r}) = \nabla \mathcal{G}(\mathbf{r}, \mathbf{r}') \mathbf{m}(\mathbf{r}')$ , where  $\mathbf{r}'$  is the position of the source dipole. A target dipole (*i.e.*, an enzyme) of length  $\ell_0$  subjected to this flow will experience an internal stress (tension or compression) proportional to the velocity gradient along its axis. This dipole-dipole force  $F_H$  will therefore be proportional to the second derivatives of the mobility,  $F_H \sim \eta w \ell_0 \nabla \nabla \mathbf{v} \sim \eta w \ell_0 m \nabla \nabla \mathcal{G}$ , where  $w$  is the hydrodynamic diameter of the dipole's beads and  $\eta$  the viscosity (see *Methods* for a detailed derivation). As biological flows are typically of low Reynolds number,  $\mathcal{G}$  can be approximated as the Oseen's tensor which scales  $\mathcal{G} \sim 1/(\eta r)$ , where  $r$  is dipole-dipole separation. Then,  $F_H \sim \eta \ell_0^2 m \nabla \nabla \mathcal{G} \sim \ell_0^2 m r^{-3}$  (taking  $w \sim \ell_0$ ).

Since the force dipoles are randomly positioned and oriented, ensemble or time averaging forbids the accumulation of net mean dipole moment,  $\langle \mathbf{m}_i(t) \rangle = 0$ . Thus, the average net flow and induced internal forces also vanish,  $\langle \nabla v \rangle \sim \langle F_H \rangle = 0$ . What survives averaging are of course the fluctuations experienced by the target dipole (the enzyme),  $\langle (\nabla v)^2 \rangle \sim \langle F_H^2 \rangle \neq 0$ . Summed over the random ensemble,

the force fluctuations scale as

$$\begin{aligned} \langle F_H^2 \rangle &\sim c_0 \langle m^2 \rangle \ell_0^4 \int_{\ell_0}^{\infty} r^{-6} d^3r \\ &\sim c_0 \ell_0 \langle m^2 \rangle \sim \mathcal{R}^{-3} \ell_0 \langle m^2 \rangle, \end{aligned} \quad (1)$$

where  $\mathcal{R} \equiv c_0^{-1/3}$  is the average dipole-dipole separation. The exact expression, derived in *Methods*, includes a geometric factor of order unity. Eq. (1) preserves the long-range nature of hydrodynamic fluctuations which decay as  $c_0 \sim \mathcal{R}^{-3}$ . For typical concentrations of active sources, such as enzymes or motors, ranging between  $c_0 \sim 1 \mu\text{M} - 1 \text{mM}$ ,  $\mathcal{R} \sim 10 - 100 \text{ nm}$ . The dipole moment fluctuation can be approximated as  $\langle m^2 \rangle \sim (\mathcal{F} \ell)^2$ , where  $\ell$  the size of the active elements and  $\mathcal{F}$  is the net force they generate during their turnover cycle. For values typical to motor proteins,  $\mathcal{F} \sim 1 \text{ pN}$  and  $\ell \sim 5 \text{ nm}$  [13, 37, 84], the dipole fluctuations would be  $\langle m^2 \rangle \sim 1 (\text{k}_B \text{T})^2$ . We shall use the value of hydrodynamic fluctuation  $\langle F_H^2 \rangle$  as the strength of the active noise.

The sources of active noise in the cell have widely varied correlation timescales, and are interdependent components of an intertwined biochemical circuitry. However, the timescales of the network's collective dynamics are much longer than the correlation time of a single source. As suggested by recent experimental measurements [9–11, 13, 85], the sources might be assumed as independent stochastic processes with intermittent bursts of activity, each with its own auto-correlation statistics. Thus, we consider the background flow as an active noise  $\zeta_A(t)$  with a characteristic correlation time  $\tau_A$  realised as:

$$\langle \zeta_A(t) \zeta_A(t') \rangle = \langle F_H^2 \rangle \exp(-|t - t'|/\tau_A). \quad (2)$$

Such activity maintains a certain type of fluctuation-dissipation relation, as observed in cells, [11, 66, 85] where injection (extraction) of an energy  $\mathcal{A}$  into (from) the system is compensated by the correlation time such that the noise strength,  $\langle F_H^2 \rangle = \mathcal{A}/\tau_A$  remains constant. With these considerations, we now proceed to derive the reaction rate theory in the presence of such active noise.

**Reaction with hydrodynamic fluctuations.** We start by writing down the dynamical equation for a catalytic process occurring in an energy landscape under the influence of a noise  $\zeta_T(t)$  of thermal origin, and an active noise  $\zeta_A(t)$  resulting from the long-range correlated hydrodynamic fluctuations,

$$\gamma \dot{q} = F(q) + \zeta_T(t) + \zeta_A(t). \quad (3)$$

The first term on the right hand side of Eq. (3) is a conservative force,  $F(q) = -\partial_q U(q)$ , exerted by the potential  $U(q) = -(a/2)q^2 + (b/4)q^4$ . The potential  $U(q)$  is made of two wells, positioned symmetrically at  $q_0 = \pm \sqrt{a/b}$  and separated by an energy barrier  $E_B = a^2/(4b)$  at  $q = 0$ . The barrier may represent, for example, conformational transitions that occur during the catalytic cycle, as recently reported in

ADK [47]<sup>1</sup>. The parameters  $a, b > 0$  are phenomenological constants. Physically,  $a$  would represent the stiffness of a protein, roughly the “spring constant” of the force dipole and  $b$  stands for the strength of the simplest possible anharmonicity that yields an activation barrier  $E_B$ . The internal friction of the landscape  $\gamma$  sets the intrinsic timescale  $\tau_0 = \gamma/a$

The thermal force  $\zeta_T(t)$  is drawn randomly from temporally uncorrelated white noise,  $\langle \zeta_T(t)\zeta_T(t') \rangle = 2\gamma k_B T \delta(t-t')$  with the noise strength fixed by the temperature  $T$ , where  $k_B$  is the Boltzmann constant. Unlike the thermal noise, the active noise  $\zeta_A(t)$  is temporally correlated (Eq. (2)), which we ensure by modelling it with an Ornstein-Uhlenbeck type evolution dynamics [86]:

$$\tau_A \dot{\zeta}_A = -\zeta_A + \sqrt{2\mathcal{A}} \xi_W(t), \quad (4)$$

where  $\xi_W(t)$  is a standard white noise process. Our main objective is to study the effect of active noise  $\zeta_A$  (with thermal noise  $\zeta_T$  in the background) on the reaction rate,  $\kappa = 1/(2\tau_{\text{MFP}})$ , where  $\tau_{\text{MFP}}$  is the mean first passage time needed to cross the energy barrier.

To gain some intuition, we examine the asymptotic case of negligible thermal noise. Then, Eqs. (3,4), can be recast as an underdamped Langevin equation,

$$(\gamma\tau_A)\ddot{q} = -\Gamma(q)\dot{q} + F(q) + \sqrt{2\mathcal{A}} \xi_W(t), \quad (5)$$

with the effective friction coefficient  $\Gamma(q) \equiv \gamma - \tau_A \partial_q F(q)$ . A remarkable feature of this nonlinear dynamical equation is that the evolution of reaction depends, besides on the force  $F(q)$  itself, also on its gradient, that is the *curvature* of the

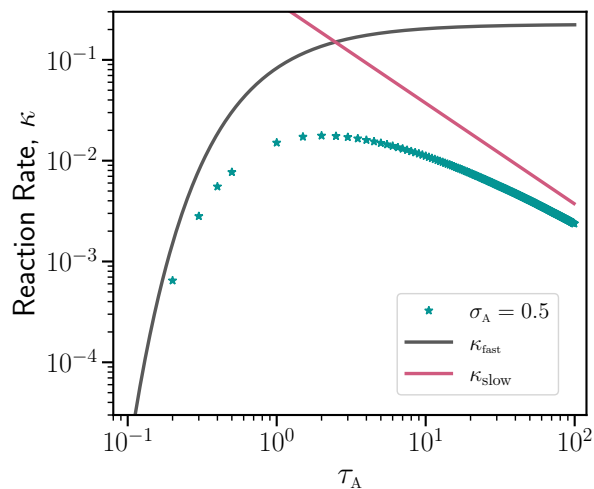


FIG. 1. Variation of reaction rate  $\kappa$ , for pure active noise of strength  $\sigma_A = 0.5$ .  $\kappa$  follows the asymptotic limits  $\kappa_{\text{slow}}$  (Eq. (7), red curve) and  $\kappa_{\text{fast}}$ , (Eq. (8), black curve).

potential,  $\partial_q F = -\partial_q^2 U$ . Thus, when  $\tau_A > \tau_0$ , the effective friction  $\Gamma(q)$  turns negative close to the energy barrier [87–90]. The negative friction region—where the motion is accelerated past the barrier—grows with  $\tau_A$ , until it stretches between the two inflection points of the potential,  $|q| \leq q_0/\sqrt{3}$ , for  $\tau_A \gg \tau_0$ . The maximal force,  $F_{\text{max}} = (2/\sqrt{3})^3 (E_B/q_0)$ , would be experienced at these inflection points. In the long-memory regime,  $\tau_A \gg \tau_0$ , any force  $F \geq F_{\text{max}}$ , is likely to push the reaction to the other potential well by crossing into the negative friction region. Thus,  $F_{\text{max}}$  sets an effective *force barrier*, similar to the energy barrier  $E_B$  in the short-memory regime. As this phenomenology evidently affects the reaction rate, we first investigate its asymptotic limits.

To this end, we turn the Langevin equation (Eq. 4) into the corresponding Fokker-Plank equation for the probability distribution  $P(q, v, t)$ , where  $v = \dot{q}$  is the velocity:

$$\frac{\partial P}{\partial t} + v \frac{\partial P}{\partial q} + \frac{F(q)}{\gamma\tau_A} \frac{\partial P}{\partial v} = \frac{\mathcal{A}}{\tau_A^2} \frac{\partial^2 P}{\partial v^2} + \frac{\Gamma(q)}{\gamma\tau_A} \frac{\partial}{\partial v} (vP). \quad (6)$$

For an active noise with long correlation time,  $\tau_A \gg \tau_0$  and strength  $\langle F_H^2 \rangle \ll F_{\text{max}}^2$ ,

$$\kappa_{\text{slow}} \simeq (2\tau_A)^{-1} \exp \left[ -\frac{1}{2} F_{\text{max}}^2 / \langle F_H^2 \rangle \right]. \quad (7)$$

This behaviour is specific to the active noise realisation which relies on  $F_{\text{max}}$  and is markedly different from purely thermal reaction rate which depends on  $E_B$ . The importance of  $F_{\text{max}}$  in the case of “slow” background has been noted in a few other recent investigations [91–93]. For the case of “fast” background,  $\tau_A \ll \tau_0$  and  $\mathcal{A} \ll \gamma E_B$ , the active noise merely scales the energy barrier and the reaction rate follows the well-known thermal behaviour,

$$\kappa_{\text{fast}} \simeq \left( \sqrt{2} \pi \tau_0 \right)^{-1} \exp \left[ -\gamma E_B / \mathcal{A} \right]. \quad (8)$$

We note that while  $\kappa_{\text{fast}}$  grows with  $\mathcal{A}$ , *i.e.*, with  $\tau_A$  for a fixed noise strength,  $\kappa_{\text{slow}}$  decays monotonically with  $\tau_A$ , suggesting an intermediate time scale where  $\kappa$  is optimal. Numerical simulations of the catalytic dynamics for pure active noise confirms this behavior (Fig 1).

As the semi-analytic Eqs. (7,8) are only valid at the asymptotic limits which are impractical to realize for enzymes, we now move on to solve Eqs. (3,4) numerically to investigate the effect of both active and thermal noise on the reaction rate. We measure the simulation time and length in units of  $\tau_0$  and  $q_0$ , respectively. Thermal and active fluctuations are also scaled by the relevant force scale as:  $\sigma_T^2 = k_B T / (2E_B)$ ,  $\sigma_A^2 = \langle F_H^2 \rangle / (4aE_B)$ . In the next section, we present behaviour of  $\kappa$  in the  $\{\sigma_A, \tau_A\}$  plane spanning over orders of magnitude. Specifically, for each point in the  $\{\sigma_A, \tau_A\}$  plane, we generate  $10^5$  independent reaction trajectories starting from an initial position chosen randomly around  $q_0$  and evolve the trajectories till it reaches  $q = 0$  where the energy barrier is maximum. The reaction rate  $\kappa$  is then computed as inverse of the mean time taken by trajectories to cross the barrier.

<sup>1</sup> Note that Eq. (3)) merely assumes that the catalytic cycle is amenable to stochastic active noise, as it is to thermal noise, but requires no coupling of reaction and conformational coordinates.

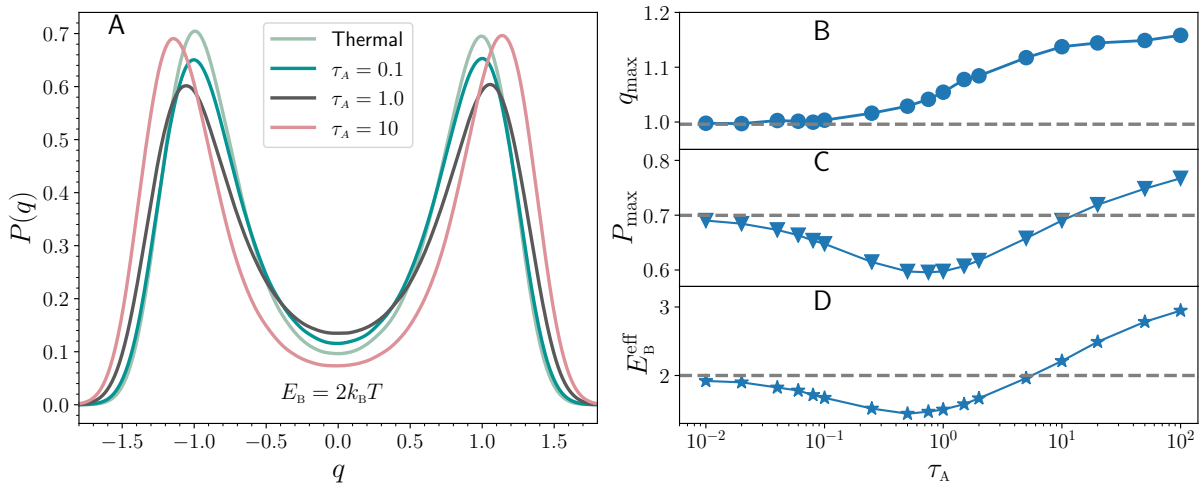


FIG. 2. Statistical features of the dynamics are presented for an energy barrier  $E_B = 2k_B T$  (*i.e.*,  $\sigma_T = 0.5$ ), and active noise strength  $\sigma_A = 0.5$ . (A) The probability density  $P(q)$  in the energy landscape for  $\tau_A = 0.1, 1.0$  and  $10.0$ . A purely thermal case is shown for reference. (B) The most probable position in the energy landscape  $q_{\max}$  is monotonically pushed away from the barrier, as compared to a purely thermal system whose maximum is at  $q = q_0$  (dashed line). (C) However, the maximal probability  $P_{\max}$  exhibits a non-monotonic dependence on  $\tau_A$ . For very small  $\tau_A$ ,  $P_{\max}$  is lower than its expected thermal value (dashed line), and continues to decrease till  $\tau_A \sim 1$ , and then turns to increase and eventually becomes larger than the thermal value. (D) Similar non-monotonic behavior of the effective energy barrier  $E_B^{\text{eff}}$ , computed from the distribution (see text). Note that, for  $\tau_A > \tau^c$ ,  $E_B^{\text{eff}}$  is larger than the purely thermal case.

## RESULTS

**Enhancement of reaction rate under active noise.** Active noise changes the magnitude of the overall force that a reaction experiences in a given energy landscape. It also changes the persistence of the force direction by introducing a correlation timescale that is absent in purely thermal agitation. As a result of this combined effect, the reaction rate  $\kappa$  is expected to change. To investigate, we consider a case where thermal and active noise have equal strength:  $\sigma_A = \sigma_T = 0.5$ , and plot  $P(q)$ , the probability distribution of the trajectories in the energy landscape, for different values of  $\tau_A$  along with the purely thermal case. (Fig. 2A) Note that the probability of forming reactant-substrate activated complex,  $P(q = 0)$ , is larger than the thermal case for  $\tau_A \sim \tau_0$  but becomes smaller for  $\tau_A = 10\tau_0$ . Following the position of the most probable value  $q_{\max}$  as a function of increasing  $\tau_A$ , we find that  $q_{\max}$  gradually moves outwards from its thermal equilibrium position  $q_{\max} = q_0$  (Fig. 2B). The movement is more rapid over an intermediate range of  $\tau_A$  while for small  $\tau_A$ ,  $q_{\max}$  mostly stays close to  $q_0$  and at large  $\tau_A$ , it somewhat settles at a certain value of  $q$ . However, the maximum value of the probability  $P_{\max}$  drops below its thermal value even when an active noise with tiny correlation is introduced (Fig. 2C).  $P_{\max}$  continues to decrease for  $\tau_A \sim \tau_0$ . As the correlation time of the active noise grows longer than the thermal crossing time, the memory of active noise start to affect the reaction adversely. The reaction trajectories now stays away from the barrier for longer time causing  $P_{\max}$  to increase. Eventually  $P_{\max}$  becomes larger than its pure thermal counterpart for active noise with  $\tau_A \gtrsim 10\tau_0$ .

The variation of  $P_{\max}$  indicates that the active noise af-

fects the reaction by *effectively* modifying the energy barrier. To confirm this, we construct an effective potential from the probability distribution as:  $V(q) = -\ln[P(q)/P(0)]$ , and compare the effective barrier  $E_B^{\text{eff}} \equiv V(0) - V(q_{\max})$  with the thermal barrier. A decrease in  $E_B^{\text{eff}} (< E_B)$  is clearly observed for small and intermediate  $\tau_A$  (Fig. 2D), where enhancement of  $\kappa$  is naturally expected. While  $E_B^{\text{eff}}$  traces the same non-monotonic behaviour of  $P_{\max}$ , it helps us to identify a crossover timescale  $\tau^c$  above which  $E_B^{\text{eff}} > E_B$ , and the reaction becomes even slower than a pure thermal case. Thus,  $\tau^c$  provides us a natural threshold to discern between “fast” ( $\tau_A < \tau^c$ ) and “slow” ( $\tau_A > \tau^c$ ) active noise, *i.e.*, the background hydrodynamic fluctuations.

Next, we examine the effect of the active noise strength  $\sigma_A$  on the reaction rate  $\kappa$ . We find that  $\sigma_A$  enhances the effect of  $\tau_A$  on  $\kappa$  as we plot it relative to the thermal reaction rate  $\kappa_T$  as a function of the scaled correlation time  $\tau_A/\tau^c$  (Fig. 3A). Evidently,  $\kappa$  becomes faster against the “fast” background and slower against the “slow” background. Note that  $\tau^c$  increases with  $\sigma_A$  (Fig. 3A Inset), demonstrating that larger  $\sigma_A$  allows a longer window of  $\tau_A$  for reaction rate enhancement.

Most importantly, it is possible to find an optimal correlation time  $\tau_A^*$  for which the enhancement of reaction rate is maximum. This maximum reaction rate  $\kappa^*$  is denoted by a  $\star$  for each  $\sigma_A$  value in Fig. 3A. Notice that the enhancement of  $\kappa$  is possible for even a tiny value of  $\sigma_A$  (Fig. 3C), but that would require a relatively larger optimal correlation time  $\tau_A^*$  (Fig. 3D, also see Fig. 5). Still,  $\tau_A^*$  is smaller than  $\tau^c$  by at least one order-of-magnitude, as rate enhancement can only occur in the presence of a fast hydrodynamic background. More enhancement is observed with increasing  $\sigma_A$  as  $\kappa^*$  grows in a scale-free fashion with  $\sigma_A > 1$ . Corre-

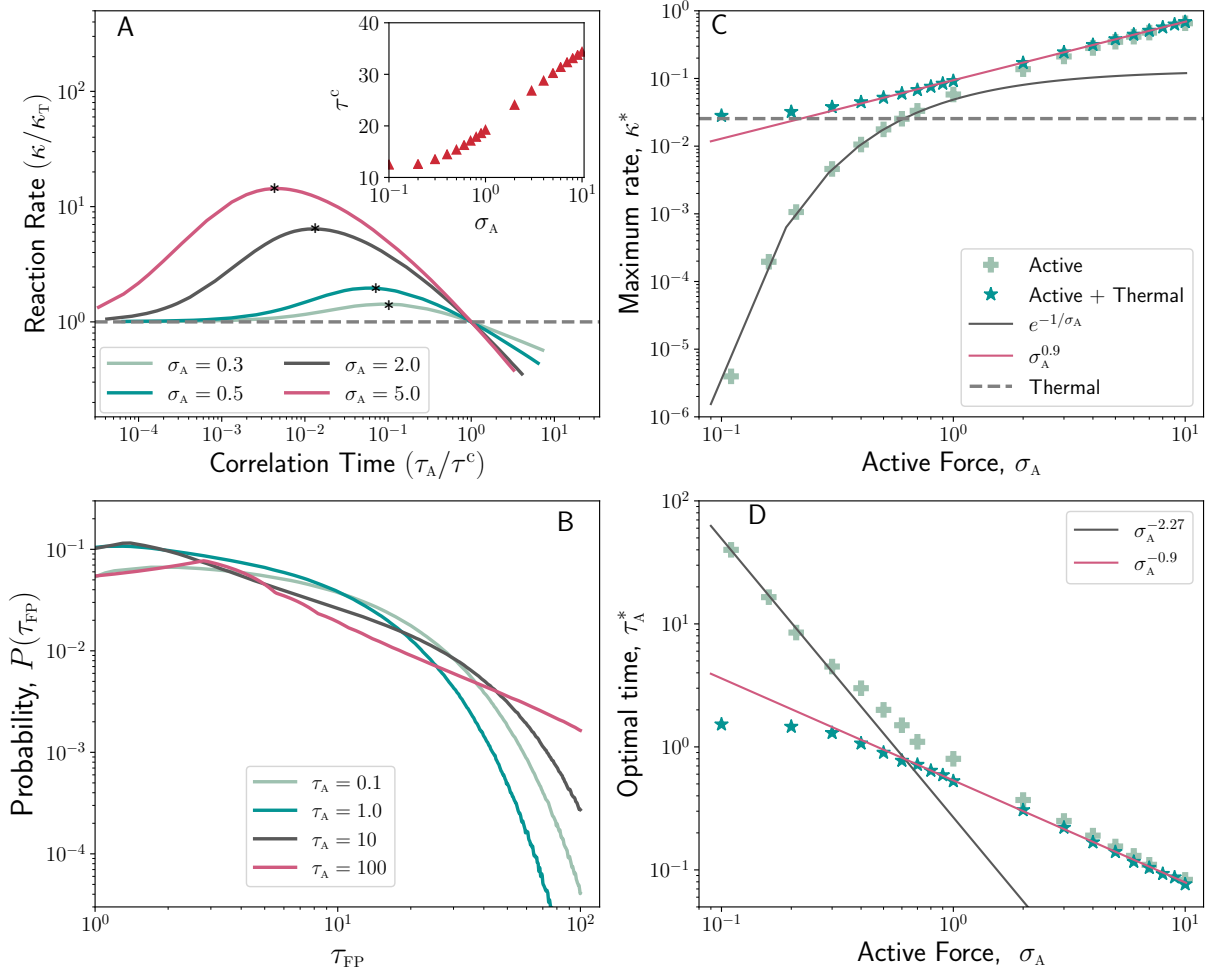


FIG. 3. (A) The effect of active noise strength  $\sigma_A$  on reaction rate  $\kappa$  for a fixed barrier  $E_B = 2k_B T$ . The variation of  $\kappa$  relative to thermal reaction rate  $\kappa_T$  for different values of  $\sigma_A$  is plotted as a function of  $\tau_A$  scaled by  $\tau^c$  (defined in the text). Dependence of  $\tau^c$  on  $\sigma_A$  is shown in the inset. For each value of  $\sigma_A$ , the maximum reaction rate  $\kappa^*$  is pointed by a  $\star$ . (B) Distribution of first passage time  $P(\tau_{FP})$ , exponential for small  $\tau_A$ , starts to grow a prominent power-law tail with increasing  $\tau_A$  indicating departure from equilibrium. (C) The maximal rate  $\kappa^*$  (stars) is never less than  $\kappa_T$  (dashed line) and increases monotonically with the active noise  $\sigma_A$ . Also shown are the rates in a purely active system (crosses). (D) The optimal correlation time  $\tau_A^*$  associated with the maximal rate  $\kappa^*$  (stars) shows a monotonic decrease with noise strength  $\sigma_A$ . Also shown is the purely active case (crosses). The numerical fits in (C) and (D) (black and red lines) are empirical functions described in the legends.

spondingly,  $\tau_A^*$  decreases in a similar fashion. As an aside, we mention that similar behavior is also expected when the active noise is much stronger than the thermal one and solely dictates the reaction. In this case,  $\kappa^*$  would decrease exponentially for small  $\sigma_A < 1$ , markedly different than the more realistic scenario of enzymatic catalysis governed by both thermal and active noise.

The non-monotonic behavior of  $\kappa$  (Fig. 3A) is the outcome of the interplay of two competing effects. First, the dynamics changes as fluctuations cross over from a fast to a adiabatic regime. To understand this effect, note that reaction dynamics in the presence of active noise can be considered as motion within a fluctuating energy landscape,  $U^{\text{eff}}(q, t) = U(q) - q\zeta_A(t)$ , with a fluctuating effective energy barrier  $E_B^{\text{eff}}(t) \simeq E_B + q_0\zeta_A(t)$  (akin to Bell's law [94]). The per-

sistence of the fluctuations is controlled by correlation time  $\tau_A$ . When the fluctuations of the landscape are much faster than the enzymatic timescale,  $\tau_A \ll \tau_0$ , the enzyme experiences an average effective barrier,  $\langle E_B^{\text{eff}} \rangle = E_B$ , and the resulting rate is  $\kappa \sim \exp(-\langle E_B^{\text{eff}} \rangle) = \exp(-E_B) \sim \kappa_T$ , *i.e.*, close to the thermal rate. But when the fluctuations become more persistent, they approach an adiabatic regime,  $\tau_0 < \tau_A < 1/\kappa_T$ , where each crossing event occurs in a practically static potential and effective barrier. In this regime, the average rate will be the average over the static potentials,  $\kappa \sim \langle \exp(-E_B^{\text{eff}}) \rangle \geq \exp(-\langle E_B^{\text{eff}} \rangle)$ , which is always larger than the rate in the fast regime<sup>2</sup>, thus explaining the increas-

<sup>2</sup> This follows from the convexity of the logarithm function,

ing part of the curve. The second effect occurs in the large correlation limit, when  $\kappa$  is controlled by the maximum force,  $F_{\max}$  rather than the activation barrier. Then, the reaction rate  $\kappa$  exhibits an inverse dependence on  $\tau_A$  (Eq. (7)), due to slowing down by the increasing effective friction,  $\Gamma(q) \sim \tau_A$  in Eq. (5).

Interpolating these two limits, one expects an optimal correlation time, where the reaction rate attains a maximum as indeed shown in the simulations. These observations agree with the computed distribution of first passage time,  $P(\tau_{\text{FP}})$ , the time taken to cross reaction barrier (Fig. 3(B)). The  $P(\tau_{\text{FP}})$  distribution follows a non-monotonic dependence similar to that of  $\tau_{\text{MFP}}$ . For  $\tau_A \sim \tau_0$ , the  $P(\tau_{\text{FP}})$  shifts to shorter  $\tau_{\text{FP}}$  values compared to the thermal regime ( $\tau_A \ll \tau_0$ ), resulting in increasing reaction rate. On the other hand, for  $\tau_A \gg \tau_0$ , the distribution shifts toward the longer first passage times, indicating slowing down compared to the thermal rate  $\kappa_T$ . Interestingly,  $P(\tau_{\text{FP}})$  crosses over from exponential scaling in the fast regime to power law behaviour in the slow regime, signaling a transition for equilibrium to nonequilibrium behavior.

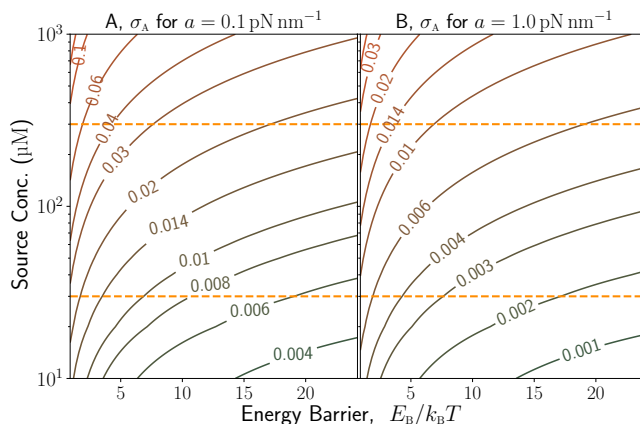


FIG. 4. Variation of scaled active force strength  $\sigma_A$  as a function of source dipole concentration  $c_0$  and barrier height  $E_B/k_B T$ . (A) and (B) corresponds to the protein stiffness values  $a = 0.1$  and  $1.0$  pN/nm, respectively. Solid curves are constant force contours, and the dashed lines denote the concentration range,  $30\text{--}300$   $\mu\text{M}$ , which is reasonably accessible in experiments.

**The case of enzymes.** Finally, we turn to the enzymatic catalysis in the presence of a fluctuating hydrodynamic background realised as a source of active noise. We choose a parameter space,  $\{\sigma_A, \tau_A\}$ , to match the experimentally realisable conditions. The scaled active noise strength,  $\sigma_A = \sqrt{\langle F_H^2 \rangle} / (4aE_B)$ , depends on the energy barrier  $E_B$ , enzyme stiffness  $a$ , and the density of the background through  $\langle F_H^2 \rangle$  as in Eq. (1). Catalytic energy barriers are measured to typically lie within a range of  $E_B = 4\text{--}24$   $k_B T$  [7, 95] and the

typical stiffness of enzymes is reported to vary within a range  $a = 0.1\text{--}1.0$  pN/nm [96–99]. In Fig. 4, we have charted out the variation of  $\sigma_A$  over a wide range of backgrounds with density ranging between  $10\text{--}1,000$   $\mu\text{M}$  as a function of  $E_B$  for two limiting values of  $a$ . As a prototypical example, consider the well-studied enzyme adenylate kinase (ADK) [43, 44]. The energy barrier  $E_B$  of ADK at room temperature is about  $10$   $k_B T$  [46]. Taking a rest length  $\ell_0 \simeq 5$  nm and internal viscosity of  $\eta \simeq 10^{-2}$  Pa s [100, 101], we obtain the friction coefficient,  $\gamma \simeq 3\pi\eta\ell_0 \simeq 10^{-10}$  kg/s, which sets the thermal timescale  $\tau_0 = \gamma/a \simeq 1$   $\mu\text{s}$  with  $a = 0.1$  pN/nm. Now we compute the reaction rate for our test enzyme over a range of  $\sigma_A$  and  $\tau_A$  for two different energy barriers,  $E_B = 6$   $k_B T$  (Fig. 5A) and  $E_B = 10$   $k_B T$  (Fig. 5B). For both cases, a red dashed line is drawn to mark the boundary between the “fast” background (on the left) and “slow” background (on the right). Within the “fast” regime, we always find an enhancement over the thermal reaction rate,  $\kappa/\kappa_T > 1$ . As a crowded solution of dipoles would correspond to a concentration,  $(1/\ell_0^3) \simeq 10$  mM, we consider a moderate regime of  $30\text{--}300$   $\mu\text{M}$ . Using the active force map in Fig. 4, we find that an enzyme is expected to experience a maximal active force,  $\sigma_A \simeq 0.003\text{--}0.03$  (shown as a horizontal dashed line in Fig. 5) over the relevant energy scale,  $E_B = 6\text{--}10$   $k_B T$ . At this limit, we see a maximum enhancement of 15% for  $E_B = 6$   $k_B T$  ( $\kappa/\kappa_T \simeq 1.15$ ) and of 50% for  $E_B = 10$   $k_B T$  ( $\kappa/\kappa_T \simeq 1.5$ ). Thus, for these typical parameters, we expect a maximum of 50% enhancement in the reaction rate.

## CONCLUSION

In summary, we have shown how a fluctuating hydrodynamic background might affect an enzymatic catalysis. Hydrodynamic fluctuations of various origins are considered as an outcome of the stochastic oscillations of a random distribution of force dipoles. Coupled through the flow they generate, these force dipoles can be collectively realised as a temporally-correlated athermal noise representing the background activity. Modelling active noise as an Ornstein-Uhlenbeck process and numerically solving reaction rate theory, now in presence of both thermal and active noise, reveals a special correlation time  $\tau^c$ , above which reaction rate start to slow down compared to the bare thermal rate.  $\tau^c$  is of the same order as inverse of thermal reaction rate  $\kappa_T$  (red dashed line in Fig. 5). Further, we find that while a slow background,  $\tau^c < \tau_A$ , somewhat slows down the catalytic activity, a faster background,  $\tau_A < \tau^c$ , always enhances the catalytic reaction rate relative to the purely thermal case. For example, a suitable choice of active noise may result in up to 50% enhancement for the typical example of ADK. We note that the present model assumes Oseen’s far-field approximation for the mobility tensor, and should be modified for densely packed sources. Once the hydrodynamic interaction is corrected to account for near-field effects, our dynamical equations can be solved for in this limit of intense active force.

The proposed physical scenario and the predicted effect of active noise on enzymatic catalysis require cautious exami-

$$\langle -E_B^{\text{eff}} \rangle = \langle \log [\exp(-E_B^{\text{eff}})] \rangle \leq \log \langle \exp(-E_B^{\text{eff}}) \rangle.$$

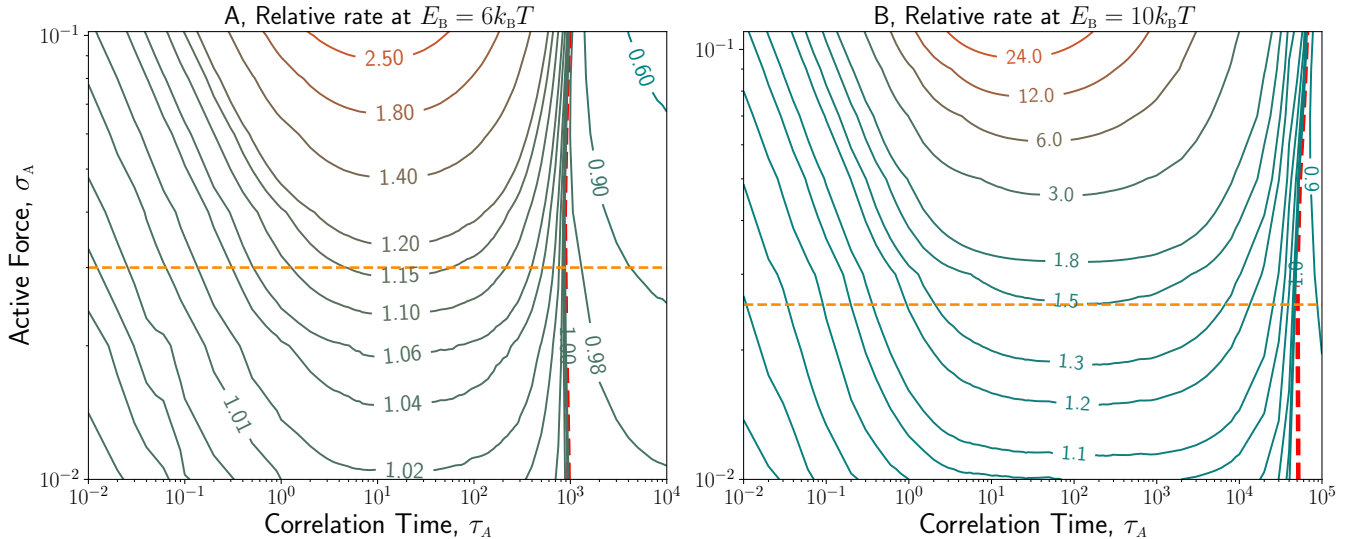


FIG. 5. The effect of active noise on the catalytic rate of an enzyme. Variation of reaction rate  $\kappa$ , relative to thermal reaction rate  $\kappa_T$ , as a function of active noise strength  $\sigma_A$  and its correlation time  $\tau_A$ , for  $E_B = 6k_B T$  (A) and  $E_B = 10k_B T$  (B). The red dashed contour marks the line where  $\kappa = \kappa_T$ , even in the presence of active fluctuations. This line separates the *slow* (right) and the *fast* (left) background regimes. Fast background always promotes enhancement of  $\kappa$ , which can be quite substantial depending on the control parameters. In contrast, slow background somewhat decelerates the reaction but not as spectacularly as in the fast background regime. For enzymatic solutions of concentration  $30\text{--}300\ \mu\text{M}$ ,  $\sigma_A$  varies between  $0.003\text{--}0.03$ . Within this range, a maximum enhancement of  $\kappa$  up to 15% is expected for  $E_B = 6k_B T$  (A) and up to 50% for  $E_B = 10k_B T$  (B).

nation. As controlling the background is hard *in vivo*, we propose a simple *in vitro* experimental test: Consider a solution consisting of two enzymes and their respective substrates in an appropriate buffer. Importantly, the two reactions are chemically orthogonal to avoid any cross-talk. The “source” enzymes generating the active noise are relatively dense to allow strong impact on the “target” enzymes, which are dilute to avoid confounding inverse effects. The active noise correlation time is approximated as the inverse thermal reaction rate of the source enzyme,  $\tau_A \simeq 1/\kappa_T^{\text{source}}$ . Also, notice that the crossover time  $\tau^c$  remains of the order of the thermal  $\tau_{\text{MFP}}$  of the target enzyme,  $\tau^c \simeq 1/\kappa_T^{\text{target}}$  (red dashed line in Fig. 5). Thus,  $\kappa_T^{\text{source}} > \kappa_T^{\text{target}}$ , implies that the source serves as fast background,  $\tau_A < \tau^c$ , and we expect an enhancement in the reaction rate of target enzyme. Conversely,  $\kappa_T^{\text{source}} < \kappa_T^{\text{target}}$ , implies a source that serves as a slow background,  $\tau_A > \tau^c$ , and is expected to slow down the rate of target enzyme. In both cases, there must be a *separation of timescales* between the target enzyme ( $\tau^c$ ) and the active noise ( $\tau_A$ ) to obtain a measurable effect on the reaction rate of target enzymes. As a consequence, a solution of only one enzyme, which serves as both target and source ( $\tau_A \simeq 1/\kappa_T^{\text{source}} = 1/\kappa_T^{\text{target}} \simeq \tau^c$ ), is expected to show no self-enhancement or self-reduction of the rate as concentration varies. The present model should in principle be applicable to other biologically relevant processes such as unzipping of DNA hairpins [77–79] for which the reported energy [80] and timescales [81] lie within the range explored in the current study.

The complex cellular environment is dense in entangled energetic processes. A fast-growing bacterium consumes energy

at a power of  $\sim 10^8 k_B T/s$ , over a volume of  $\sim 1\ \mu\text{m}^3$  [84]. In the eukaryotic cell, there are high-activity regions and organelles, such as mitochondria and chloroplasts, where the proposed effects might be significant. One may speculate that molecular motors, whose turnover rate is relatively slow [36, 84], can be accelerated in the presence of high metabolic activity. To treat such elaborate scenarios, we plan to further extend the present bare-bone model to include the causal dependence of reactions in a network and the spatiotemporal heterogeneity of the embedding background. We hope the current results would stimulate further study of potential effects of active stochastic environment on biochemical processes.

## METHODS

**Hydrodynamic forces induced by active processes.** We consider a solution of stochastic force dipoles [64, 70] representing active processes such as enzymatic catalysis and the motion of molecular motors. In this coarse-grained view, each force dipole consists of two beads connected by a spring of equilibrium length  $\ell_0$ . The beads represent the domains of the enzyme that move with respect to each other during the catalysis. Consider a collection of force dipoles  $\{\mathbf{m}_i\}$  located at positions  $\{\mathbf{R}_i\}$  with random independent orientations  $\{\mathbf{e}_i\}$  (3D unit vectors). Our target dipole has its two domains (*i.e.*, spheres) located at positions  $\mathbf{R}$  and  $\mathbf{R}' = \mathbf{R} + \ell\mathbf{e}$ , with an orientation  $\mathbf{e}$  and distance  $\ell = |\mathbf{R}' - \mathbf{R}|$ . Following Mikhailov

and Kapral [70], we find the velocities  $\dot{\mathbf{R}}$  of the domains—using the mobility tensor  $\mathcal{G}_{\alpha\beta}$ —by summing the contributions of the velocity fields induced by the surrounding dipoles,

$$\dot{R}_\alpha = \sum_i^N \frac{\partial \mathcal{G}_{\alpha\beta}(\mathbf{R} - \mathbf{R}_i)}{\partial R_{i\mu}} e_{i\beta} e_{i\mu} m_i(t), \quad (9)$$

$$\dot{R}'_\alpha = \sum_i^N \frac{\partial \mathcal{G}_{\alpha\beta}(\mathbf{R}' - \mathbf{R}_i)}{\partial R_{i\mu}} e_{i\beta} e_{i\mu} m_i(t), \quad (10)$$

where the Greek indices denote  $x, y, z$  components of vectors and tensors, and we follow Einstein's convention of summation over repeated indices. The mobility tensor  $\mathcal{G}_{\alpha\beta}$  is the *Green function* of the linear Stokes flow, which yields the velocity field resulting from a localized force [102]. Eq. (10) involves spatial derivatives of  $\mathcal{G}$ , which are the Taylor expansions around each force dipole.

The time-dependent dipole moment exerted on the target  $m(t)$  is  $m(t) = \ell(t)F(t)$ , where  $\ell(t)$  and  $F(t)$  are the distance and interaction force between the two domains. Thus, for a target enzyme of length  $\ell(t)$ , the relative velocity  $\delta v$  between the two domains is given by

$$\delta v_\alpha = \dot{R}'_\alpha - \dot{R}_\alpha = \sum_i^N e_{i\beta} e_{i\mu} m_i(t) \left[ \frac{\partial \mathcal{G}_{\alpha\beta}(\mathbf{R} + \ell(t)\mathbf{e} - \mathbf{R}_i)}{\partial R_{i\mu}} - \frac{\partial \mathcal{G}_{\alpha\beta}(\mathbf{R} - \mathbf{R}_i)}{\partial R_{i\mu}} \right].$$

Since the linear extension of the enzyme  $\ell(t)$  is much smaller than the dipole-dipole distances, we can take a far-field approximation by expanding the difference to first order in  $\ell$ ,

$$\delta v_\alpha = \ell(t) \sum_i \frac{\partial^2 \mathcal{G}_{\alpha\beta}(\mathbf{R} - \mathbf{R}_i)}{\partial R_{i\mu} \partial R_\nu} e_{i\beta} e_{i\mu} e_\nu m_i(t).$$

Therefore, the relative velocity with which the spring connecting the two domains compresses or stretches is the projection

$$\delta \mathbf{v} \cdot \mathbf{e} = \ell(t) \sum_i \frac{\partial^2 \mathcal{G}_{\alpha\beta}(\mathbf{R} - \mathbf{R}_i)}{\partial R_{i\mu} \partial R_\nu} e_{i\beta} e_{i\mu} e_\nu e_\alpha m_i(t).$$

Applying Stoke's law, we find that the deformation forces acting on the target dipole is

$$F_{\text{H}}(\mathbf{R}, t) = (3\pi\eta w) (\delta \mathbf{v} \cdot \mathbf{e}) = 3\pi\eta w \ell(t) \times \sum_i \frac{\partial^2 \mathcal{G}_{\alpha\beta}(\mathbf{R} - \mathbf{R}_i)}{\partial R_{i\mu} \partial R_\nu} e_{i\beta} e_{i\mu} e_\nu e_\alpha m_i(t), \quad (11)$$

where  $w$  is the domain size (*i.e.*, its hydrodynamic diameter) and  $\eta$  the viscosity of the solution. Since enzymes are randomly oriented, then without any loss of generality, we take the target enzyme oriented along the  $x$ -axis, thereby simplifying Eq. (11) into

$$F_{\text{H}}(\mathbf{R}, t) = 3\pi\eta w \ell(t) \sum_i \frac{\partial^2 \mathcal{G}_{x\beta}(\mathbf{R} - \mathbf{R}_i)}{\partial R_{i\mu} \partial R_x} e_{i\beta} e_{i\mu} m_i(t). \quad (12)$$

Next, we rewrite Eq. (12) in a field-point notation, which will be convenient for further manipulation,

$$F_{\text{H}}(\mathbf{R}, t) = 3\pi\eta w \ell(t) \int d\mathbf{r} \frac{\partial^2 \mathcal{G}_{x\beta}(\mathbf{r})}{\partial r_\mu \partial r_x} \times \sum_i e_{i\beta} e_{i\mu} m_i(t) \delta(\mathbf{r} - \mathbf{R}_i + \mathbf{R}).$$

The mean force is proportional to the average over the sum of dipole moments, which vanishes due to the symmetry in the homogeneous isotropic solution [70],  $\langle F_{\text{H}}(\mathbf{R}, t) \rangle \sim \langle m_i(t) \rangle = 0$ . However, the second moment—that is the average squared force the target dipole experiences due to the collective fluctuations of other force dipoles—does not vanish,

$$\begin{aligned} \langle F_{\text{H}}(\mathbf{R}, t) F_{\text{H}}(\mathbf{R}, t') \rangle &= (3\pi\eta w)^2 \langle \ell(t) \ell(t') \rangle \\ &\times \int d\mathbf{r} \frac{\partial^2 \mathcal{G}_{x\beta}(\mathbf{r})}{\partial r_\mu \partial r_x} \frac{\partial^2 \mathcal{G}_{x\beta'}(\mathbf{r})}{\partial r_{\mu'} \partial r_x} \\ &\times \sum_i \langle e_{i\beta} e_{i\mu} e_{i\beta'} e_{i\mu'} \delta(\mathbf{r} - \mathbf{R}_i + \mathbf{R}) m_i(t) m_i(t') \rangle, \end{aligned}$$

Since dipole orientations are uncorrelated with their positions, the last term in above equation can be simplified,

$$\begin{aligned} \sum_i \langle e_{i\beta} e_{i\mu} e_{i\beta'} e_{i\mu'} \delta(\mathbf{r} - \mathbf{R}_i + \mathbf{R}) m_i(t) m_i(t') \rangle \\ = \langle e_\beta e_\mu e_{\beta'} e_{\mu'} \rangle \langle m(t) m(t') \rangle c(\mathbf{R} + \mathbf{r}), \end{aligned}$$

where  $c(\mathbf{r}) = \sum_i \delta(\mathbf{r} - \mathbf{R}_i)$  is the concentration of force dipoles in the solution. Thus, we find that the second moment of the force is

$$\begin{aligned} \langle F_{\text{H}}(\mathbf{R}, t) F_{\text{H}}(\mathbf{R}, t') \rangle &= (3\pi\eta w)^2 \langle \ell(t) \ell(t') \rangle \\ &\times \int d\mathbf{r} \frac{\partial^2 \mathcal{G}_{x\beta}(\mathbf{r})}{\partial r_\mu \partial r_x} \frac{\partial^2 \mathcal{G}_{x\beta'}(\mathbf{r})}{\partial r_{\mu'} \partial r_x} c(\mathbf{R} + \mathbf{r}) \\ &\times \langle e_\beta e_\mu e_{\beta'} e_{\mu'} \rangle \langle m(t) m(t') \rangle. \end{aligned}$$

Assuming a uniform concentration, the variance of this force is

$$\begin{aligned} \langle F_{\text{H}}^2(\mathbf{R}, t) \rangle &= (3\pi\eta w)^2 \langle \ell^2(t) \rangle \langle m^2(t) \rangle c_0 \\ &\times \int d\mathbf{r} \frac{\partial^2 \mathcal{G}_{x\beta}(\mathbf{r})}{\partial r_\mu \partial r_x} \frac{\partial^2 \mathcal{G}_{x\beta'}(\mathbf{r})}{\partial r_{\mu'} \partial r_x} \langle e_\beta e_\mu e_{\beta'} e_{\mu'} \rangle. \end{aligned} \quad (13)$$

Since dipolar orientation is uncorrelated, the 4-point correlation term  $\langle e_\beta e_\mu e_{\beta'} e_{\mu'} \rangle$  vanishes unless there are even powers of the components of the orientation vector  $\mathbf{e}$ . We can therefore write the 4-point correlation as a sum over products of  $\delta$ -functions,

$$\langle e_\beta e_\mu e_{\beta'} e_{\mu'} \rangle = A_d [\delta_{\beta\beta'} \delta_{\mu\mu'} + \delta_{\beta\mu} \delta_{\beta'\mu'} + \delta_{\beta\mu'} \delta_{\beta'\mu}],$$

where  $A_d = 1/15$  for a 3D system.

To proceed further, we use a far-field approximation for  $\mathcal{G}_{\alpha\beta}$  in terms of the Oseen tensor [82, 102], which for a 3D system is

$$\mathcal{G}_{\alpha\beta}(\mathbf{r}) = \frac{1}{8\pi\eta r} \left[ \delta_{\alpha\beta} + \frac{r_\alpha r_\beta}{r^2} \right]. \quad (14)$$



The Oseen approximation is valid as long as the separation between dipoles is large compared to their size. Substituting Eq. (14) in Eq. (13) and introducing a scaled coordinate  $\xi = \mathbf{r}/\ell_0$ , we find

$$\begin{aligned} \langle F_{\text{H}}^2(\mathbf{R}, t) \rangle &= \frac{9}{64} A_d \langle \ell^2(t) \rangle \langle m^2(t) \rangle c_0 w^2 \ell_0^{-3} \\ &\times \int_1^\infty d\xi \frac{\partial^2 \mathcal{G}_{x\beta}(\xi)}{\partial \xi_\mu \partial \xi_x} \frac{\partial^2 \mathcal{G}_{x\beta'}(\xi)}{\partial \xi_{\mu'} \partial \xi_x} \\ &\times (\delta_{\beta\beta'} \delta_{\mu\mu'} + \delta_{\beta\mu} \delta_{\beta'\mu'} + \delta_{\beta\mu'} \delta_{\beta'\mu}) , \end{aligned} \quad (15)$$

where the scaled Oseen tensor is  $\mathcal{G}_{\alpha\beta}(\xi) = \xi^{-1}(1 + \xi_\alpha \xi_\beta / \xi^2)$ . Since the mobility tensor diverges as  $1/\xi^3$  at small distances, we introduce a cut-off in the lower limit of the integration accounting for the finite size of the dipole (*i.e.*, enzyme). The integral in the Eq. (15) is a dimensionless factor, which depends on the derivatives of  $\mathcal{G}_{\alpha\beta}(\xi)$  and the dipole orientations. A straightforward calculation yields

$$\begin{aligned} \int_1^\infty d\xi \frac{\partial^2 \mathcal{G}_{x\beta}(\xi)}{\partial \xi_\mu \partial \xi_x} \frac{\partial^2 \mathcal{G}_{x\beta'}(\xi)}{\partial \xi_{\mu'} \partial \xi_x} \\ \times (\delta_{\beta\beta'} \delta_{\mu\mu'} + \delta_{\beta\mu} \delta_{\beta'\mu'} + \delta_{\beta\mu'} \delta_{\beta'\mu}) = \frac{96\pi}{5} . \end{aligned}$$

Finally, substituting the value of integral in Eq. (15), we find the variance of the hydrodynamic force,

$$\langle F_{\text{H}}^2(\mathbf{R}, t) \rangle = \left( \frac{9\pi}{50} \cdot \frac{w^2}{\ell_0^2} \cdot \frac{\langle \ell^2 \rangle}{\ell_0^2} \right) \left( \frac{\langle m^2 \rangle}{\ell_0^2} \right) (c_0 \ell_0^3) . \quad (16)$$

The dependence of the hydrodynamic force on the inter-dipole distance  $\mathcal{R}$  arises from the dipole concentration  $c_0 = 1/\mathcal{R}^3$ . The first three terms on the right-hand side of Eq. (16) are combined into a geometric factor  $\lambda = (9\pi/50)w^2\langle\ell^2\rangle/\ell_0^4$ . This constant is of order  $\lambda \simeq 1/2$  since all the three lengths are similar. We have used Eq. (16) to estimate the hydrodynamic force generated by an enzymatic solution.

**Barrier crossing under the combined influence of thermal and active noise.** We examine overdamped Langevin dynamics in a energy landscape  $U(q)$  of a symmetric bistable system,

$$U(q) = -\frac{a}{2}q^2 + \frac{b}{4}q^4 .$$

$U(q)$  has two minima at  $q_m = \pm\sqrt{a/b}$ , separated by an energy barrier,  $E_B = a^2/(4b)$ . In the overdamped Langevin framework, the coordinate  $q$  evolves according to

$$\gamma \dot{q} = -\frac{\partial U}{\partial q} + \zeta_{\text{T}}(t) + \zeta_{\text{A}}(t) . \quad (17)$$

The noise term  $\zeta_{\text{T}}(t)$  in Eq.[17] is a standard stochastic thermal force with the statistics

$$\langle \zeta_{\text{T}}(t) \zeta_{\text{T}}(t') \rangle = 2\gamma k_{\text{B}} T \delta(t - t') ,$$

The active force  $\zeta_{\text{T}}(t)$  is modeled as an Ornstein-Uhlenbeck Process,

$$\tau_{\text{A}} \dot{\zeta}_{\text{A}} = -\zeta_{\text{A}} + \sqrt{2\bar{\mathcal{A}}} \xi_{\text{W}}(t) , \quad (18)$$

where  $\xi_{\text{W}}(t)$  is a white noise source with zero mean and unit variance,  $\mathcal{A}$  is the energy scale of the active force, and  $\tau_{\text{A}}$  correlation time of the activity. The corresponding active force statistics is given by

$$\langle \zeta_{\text{A}}(t) \zeta_{\text{A}}(t') \rangle = (\mathcal{A}/\tau_{\text{A}}) e^{-|t-t'|/\tau_{\text{A}}} .$$

For an Ornstein-Uhlenbeck process, the fluctuation-dissipation relation implies that  $\mathcal{A}$  is proportional to  $\tau_{\text{A}}$ . Hence, the variance of the active force,  $\langle F_{\text{H}}^2 \rangle = \langle \zeta_{\text{A}}^2(t) \rangle = \mathcal{A}/\tau_{\text{A}}$ , remains constant.

To examine the impact of active noise on barrier crossing, we numerically solve many realizations of Eq. (17) and analyze the statistics of crossing events. For this purpose, we introduce the following scaling

$$\bar{t} = t/\tau_0 , \quad \bar{q} = q/q_0 ,$$

where  $\tau_0 = \gamma/a$  is the thermal relaxation time of the particle in the vicinity of the minimum at  $q_0$ . Using the above scaling, we obtain a dimensionless form of the Eqs. (17,18)

$$\dot{\bar{q}} = \bar{q} - \bar{q}^3 + \bar{\zeta}_{\text{T}}(\bar{t}) + \bar{\zeta}_{\text{A}}(\bar{t}) , \quad (19)$$

$$\tau_{\text{A}} \dot{\bar{\zeta}}_{\text{A}} = -\bar{\zeta}_{\text{A}} + \sqrt{2\bar{\mathcal{A}}} \xi_{\text{W}}(\bar{t}) , \quad (20)$$

with  $\bar{\mathcal{A}} = \mathcal{A}/(4\gamma E_{\text{B}})$ . The corresponding scaled noise statistics are

$$\begin{aligned} \langle \bar{\zeta}_{\text{T}}(\bar{t}) \bar{\zeta}_{\text{T}}(\bar{t}') \rangle &= \sigma_{\text{T}}^2 \delta(\bar{t} - \bar{t}') , \\ \langle \bar{\zeta}_{\text{A}}(\bar{t}) \bar{\zeta}_{\text{A}}(\bar{t}') \rangle &= \sigma_{\text{A}}^2 \exp(-|\bar{t} - \bar{t}'|/\bar{\tau}_{\text{A}}) , \\ \langle \xi_{\text{W}}(\bar{t}) \xi_{\text{W}}(\bar{t}') \rangle &= \delta(\bar{t} - \bar{t}') , \end{aligned} \quad (21)$$

where  $\sigma_{\text{A}}^2 = \langle F_{\text{H}}^2 \rangle / (4aE_{\text{B}})$ , and  $\sigma_{\text{T}}^2 = k_{\text{B}}T/(2E_{\text{B}})$  are the scaled active and thermal noise strength. Eqs. (19,20,21) are the central equations in our numerical and analytical study. To simplify the notation, we will hereafter omit the overbar in the scaled variables (so  $q = \bar{q}$  etc.).

**The numerical simulation.** We solve Eqs. (19) employing an explicit Euler scheme [103], which yields the following iterative dynamics for the coordinate:

$$q(t + dt) = q(t)(1 + dt) - q^3(t) dt + X_{\zeta_{\text{T}}} + X_{\zeta_{\text{A}}} ,$$

where  $X_{\zeta_{\text{T}}}$  and  $X_{\zeta_{\text{A}}}$  are the random processes

$$X_{\zeta_{\text{T}}} = \int_t^{t+dt} \zeta_{\text{T}}(u) du , \quad (22)$$

$$X_{\zeta_{\text{A}}} = \int_t^{t+dt} \zeta_{\text{A}}(u) du . \quad (23)$$

The Gaussian distribution of the white thermal noise  $\zeta_{\text{T}}$  has zero mean, and a variance  $\sigma_{\text{T}}^2$ . Therefore, the distribution of  $X_{\zeta_{\text{T}}}$  is simply  $X_{\zeta_{\text{T}}} = \sqrt{dt} \sigma_{\text{T}} Y_{\text{T}}$ , where  $Y_{\text{T}} \sim \mathcal{N}(0, 1)$  is distributed according to the standard normal distribution with zero mean and unit variance.

Integrating Eq. (20), we obtain a formal solution for the active noise,

$$\zeta_{\text{A}}(t) = e^{-t/\tau_{\text{A}}} \zeta_{\text{A}}(0) + \frac{\sqrt{2\bar{\mathcal{A}}}}{\tau_{\text{A}}} \int_0^t e^{(u-t)/\tau_{\text{A}}} \xi_{\text{W}}(u) du .$$

Substitution of the latter result into Eq. (23), yields the statistics of  $X_{\zeta_A}$ . To proceed further, we define two Gaussian processes [86, 103],

$$\Omega_0 = \int_0^{dt} du e^{(u-dt)/\tau_A} \xi_w(u),$$

$$\Omega_1 = \int_0^{dt} du \int_0^u dv e^{(v-u)/\tau_A} \xi_w(v).$$

Solving these equations, we express the  $\Omega_0, \Omega_1$  processes as

$$\Omega_0 = \sqrt{\langle \Omega_0^2 \rangle} Y_0,$$

$$\Omega_1 = \frac{\langle \Omega_0 \Omega_1 \rangle}{\sqrt{\langle \Omega_0^2 \rangle}} Y_0 + \sqrt{\langle \Omega_1^2 \rangle - \frac{\langle \Omega_0 \Omega_1 \rangle^2}{\langle \Omega_0^2 \rangle}} Y_1,$$

with the correlations defined in terms of  $\mu = dt/\tau_A$  as

$$\langle \Omega_0^2 \rangle = \frac{\tau_A}{2} (1 - e^{-2\mu}),$$

$$\langle \Omega_1^2 \rangle = \frac{\tau_A^3}{2} (2\mu - 3 - e^{-2\mu} + 4e^{-\mu}),$$

$$\langle \Omega_0 \Omega_1 \rangle = \frac{\tau_A^2}{2} (1 - 2e^{-\mu} + e^{-2\mu}),$$

and  $Y_0 \sim \mathcal{N}(0, 1)$  and  $Y_1 \sim \mathcal{N}(0, 1)$  are two independent standard Gaussian processes of zero mean and unit variance. With the expressions for the stochastic processes, the time update algorithm for active noise and coordinate becomes

$$\zeta_A(t + dt) = e^{-\mu} \zeta_A(t) + \frac{\sqrt{2\mathcal{A}}}{\tau_A} \Omega_0,$$

$$q(t + dt) = q(t)(1 + dt) - q^3(t) dt + \sqrt{dt} \sigma_T Y_T$$

$$+ \tau_A (1 - e^{-\mu}) \zeta_A(t) + \frac{\sqrt{2\mathcal{A}}}{\tau_A} \Omega_1.$$

To calculate the barrier crossing rate, we consider a particle, initially positioned at the left minimum  $q = -1$  (i.e.,  $q = -q_0$ ). We then monitor the particle trajectory and find the first passage time—the time when the particle crosses the energy barrier for the first time. We repeat the process for  $10^5$  independent noise realizations and average to obtain *mean* first passage time  $\tau_{\text{MFP}}$ . In a bistable system, the reaction rate  $\kappa$  is inversely proportional to the mean first passage time,  $\kappa = \frac{1}{2} \tau_{\text{MFP}}^{-1}$ .

- 
- [1] J. Haldane, *Enzymes* (Longmans, Green and Company, 1930).
- [2] L. C. Pauling, Molecular architecture and biological reactions, *Chem Eng News* **24**, 1375 (1946).
- [3] L. C. Pauling, Chemical achievement and hope for the future, *American scientist* **36**, 51–58 (1948).
- [4] A. Warshel and M. Levitt, Theoretical studies of enzymic reactions: Dielectric, electrostatic and steric stabilization of the carbonium ion in the reaction of lysozyme, *J Mol Biol* **103**, 227 (1976).
- [5] A. Warshel, Energetics of enzyme catalysis, *Proc Natl Acad Sci* **75**, 5250 (1978).
- [6] J. Kraut, How do enzymes work?, *Science* **242**, 533 (1988).
- [7] A. Fersht, *Structure and Mechanism in Protein Science* (World Scientific, 2017).
- [8] A. Kessel and N. Ben-Tal, *Introduction to Proteins: Structure, Function, and Motion* (CRC Press, 2018).
- [9] M. Guo, A. Ehrlicher, M. Jensen, M. Renz, J. Moore, R. Goldman, J. Lippincott-Schwartz, F. Mackintosh, and D. Weitz, Probing the stochastic, motor-driven properties of the cytoplasm using force spectrum microscopy, *Cell* **158**, 822 (2014).
- [10] H. Turlier, D. A. Fedosov, B. Audoly, T. Auth, N. S. Gov, C. Sykes, J.-F. Joanny, G. Gompper, and T. Betz, Equilibrium physics breakdown reveals the active nature of red blood cell flickering, *Nat Phys* **12**, 513 (2016).
- [11] É. Fodor, W. W. Ahmed, M. Almonacid, M. Bussonnier, N. S. Gov, M.-H. Verlhac, T. Betz, P. Visco, and F. van Wijland, Nonequilibrium dissipation in living oocytes, *Europhys Lett* **116**, 30008 (2016).
- [12] C. Battle, C. P. Broedersz, N. Fakhri, V. F. Geyer, J. Howard, C. F. Schmidt, and F. C. MacKintosh, Broken detailed balance at mesoscopic scales in active biological systems, *Science* **352**, 604 (2016).
- [13] W. W. Ahmed, Étienne Fodor, M. Almonacid, M. Bussonnier, M.-H. Verlhac, N. Gov, P. Visco, F. van Wijland, and T. Betz, Active mechanics reveal molecular-scale force kinetics in living oocytes, *Biophys J* **114**, 1667 (2018).
- [14] R. H. Austin, K. W. Beeson, L. Eisenstein, H. Frauenfelder, and I. C. Gunsalus, Dynamics of ligand binding to myoglobin, *Biochemistry (Mosc)* **14**, 5355 (1975).
- [15] M. Gerstein, A. M. Lesk, and C. Chothia, Structural mechanisms for domain movements in proteins, *Biochemistry (Mosc)* **33**, 6739 (1994).
- [16] G. G. Hammes, Multiple conformational changes in enzyme catalysis, *Biochemistry (Mosc)* **41**, 8221 (2002).
- [17] R. M. Daniel, R. V. Dunn, J. L. Finney, and J. C. Smith, The role of dynamics in enzyme activity, *Annu Rev Biophys Biomol Struct* **32**, 69 (2003).
- [18] A. Gutteridge and J. Thornton, Conformational changes observed in enzyme crystal structures upon substrate binding, *J Mol Biol* **346**, 21 (2005).
- [19] D. D. Boehr, H. J. Dyson, and P. E. Wright, An nmr perspective on enzyme dynamics, *Chem Rev* **106**, 3055 (2006).
- [20] Z. D. Nagel and J. P. Klinman, A 21st century revisionist's view at a turning point in enzymology, *Nat Chem Biol* **5**, 543

- (2009).
- [21] D. R. Glowacki, J. N. Harvey, and A. J. Mulholland, Taking ockham’s razor to enzyme dynamics and catalysis, *Nat Chem* **4**, 169 (2012).
- [22] G. Bhabha, J. T. Biel, and J. S. Fraser, Keep on moving: Discovering and perturbing the conformational dynamics of enzymes, *Acc. Chem. Res.* **48**, 423 (2015).
- [23] R. Callender and R. B. Dyer, The dynamical nature of enzymatic catalysis, *Acc. Chem. Res.* **48**, 407 (2015).
- [24] A. G. Palmer, Enzyme dynamics from nmr spectroscopy, *Acc. Chem. Res.* **48**, 457 (2015).
- [25] M. R. Mitchell, T. Tlusty, and S. Leibler, Strain analysis of protein structures and low dimensionality of mechanical allosteric couplings, *Proc Natl Acad Sci USA* **113**, E5847 (2016).
- [26] D. Koshland, Application of a theory of enzyme specificity to protein synthesis, *Proc Natl Acad Sci* **44**, 98 (1958).
- [27] B. Ma and R. Nussinov, Enzyme dynamics point to stepwise conformational selection in catalysis, *Curr Opin Chem Biol* **14**, 652 (2010).
- [28] B. G. Vértessy and F. Orosz, From “fluctuation fit” to “conformational selection”: Evolution, rediscovery, and integration of a concept, *Bioessays* **33**, 30 (2011).
- [29] J. Monod, J. Wyman, and J.-P. Changeux, On the nature of allosteric transitions: A plausible model, *J Mol Biol* **12**, 88 (1965).
- [30] M. F. Perutz, Stereochemistry of cooperative effects in haemoglobin: Haem-haem interaction and the problem of allostery, *Nature* **228**, 726 (1970).
- [31] N. M. Goodey and S. J. Benkovic, Allosteric regulation and catalysis emerge via a common route, *Nat Chem Biol* **4**, 474 (2008).
- [32] H. N. Motlagh, J. O. Wrabl, J. Li, and V. J. Hilser, The ensemble nature of allostery, *Nature* **508**, 331 (2014).
- [33] K. H. DuBay, G. R. Bowman, and P. L. Geissler, Fluctuations within folded proteins: Implications for thermodynamic and allosteric regulation, *Acc. Chem. Res.* **48**, 1098 (2015).
- [34] B. P. English, W. Min, A. M. van Oijen, K. T. Lee, G. Luo, H. Sun, B. J. Cherayil, S. C. Kou, and X. S. Xie, Ever-fluctuating single enzyme molecules: Michaelis-menten equation revisited, *Nat Chem Biol* **2**, 87 (2006).
- [35] E. Campbell, M. Kaltenbach, G. J. Correy, P. D. Carr, B. T. Porebski, E. K. Livingstone, L. Afriat-Jurnou, A. M. Buckle, M. Weik, F. Hollfelder, N. Tokuriki, and C. J. Jackson, The role of protein dynamics in the evolution of new enzyme function, *Nat Chem Biol* **12**, 944 (2016).
- [36] J. Howard, Molecular motors: structural adaptations to cellular functions, *Nature* **389**, 561 (1997).
- [37] R. D. Vale, The molecular motor toolbox for intracellular transport, *Cell* **112**, 467 (2003).
- [38] N. Kodera, D. Yamamoto, R. Ishikawa, and T. Ando, Video imaging of walking myosin v by high-speed atomic force microscopy, *Nature* **468**, 72 (2010).
- [39] H. S. Muddana, S. Sengupta, T. E. Mallouk, A. Sen, and P. J. Butler, Substrate catalysis enhances single-enzyme diffusion, *J Am Chem Soc* **132**, 2110 (2010), PMID: 20108965.
- [40] K. K. Dey, X. Zhao, B. M. Tansi, W. J. Méndez-Ortiz, U. M. Córdova-Figueroa, R. Golestanian, and A. Sen, Micromotors powered by enzyme catalysis, *Nano Lett* **15**, 8311 (2015).
- [41] A.-Y. Jee, S. Dutta, Y.-K. Cho, T. Tlusty, and S. Granick, Enzyme leaps fuel antichemotaxis, *Proc Natl Acad Sci* **115**, 14 (2018).
- [42] A.-Y. Jee, Y.-K. Cho, S. Granick, and T. Tlusty, Catalytic enzymes are active matter, *Proc Natl Acad Sci* **115**, E10812 (2018).
- [43] M. Wolf-Watz, V. Thai, K. Henzler-Wildman, G. Hadjipavlou, E. Z. Eisenmesser, and D. Kern, Linkage between dynamics and catalysis in a thermophilic-mesophilic enzyme pair, *Nature Structural Molecular Biology* **11**, 945 (2004).
- [44] K. Henzler-Wildman, V. Thai, M. Lei, and et al., Intrinsic motions along an enzymatic reaction trajectory, *Nature* **450**, 838 (2007).
- [45] K. A. Henzler-Wildman, M. Lei, V. Thai, S. J. Kerns, M. Karplus, and D. Kern, A hierarchy of timescales in protein dynamics is linked to enzyme catalysis, *Nature* **450**, 913 (2007).
- [46] U. Olsson and M. Wolf-Watz, Overlap between folding and functional energy landscapes for adenylate kinase conformational change, *Nat Commun* **1**, 111 (2010).
- [47] H. Y. Aviram, M. Pirchi, H. Mazal, Y. Barak, I. Riven, and G. Haran, Direct observation of ultrafast large-scale dynamics of an enzyme under turnover conditions, *Proc Natl Acad Sci USA* **115**, 3243 (2018).
- [48] J. R. Schnell, H. J. Dyson, and P. E. Wright, Structure, dynamics, and catalytic function of dihydrofolate reductase, *Annu Rev Biophys Biomol Struct* **33**, 119 (2004).
- [49] R. P. Venkitakrishnan, E. Zaborowski, D. McElheny, S. J. Benkovic, H. J. Dyson, and P. E. Wright, Conformational changes in the active site loops of dihydrofolate reductase during the catalytic cycle, *Biochemistry (Mosc )* **43**, 16046 (2004).
- [50] D. D. Boehr, D. McElheny, H. J. Dyson, and P. E. Wright, The dynamic energy landscape of dihydrofolate reductase catalysis, *Science* **313**, 1638 (2006).
- [51] S. Hammes-Schiffer and S. J. Benkovic, Relating protein motion to catalysis, *Annu Rev Biochem* **75**, 519 (2006).
- [52] G. Bhabha, J. Lee, D. C. Ekiert, J. Gam, I. A. Wilson, H. J. Dyson, S. J. Benkovic, and P. E. Wright, A dynamic knockout reveals that conformational fluctuations influence the chemical step of enzyme catalysis, *Science* **332**, 234 (2011).
- [53] L. Y. P. Luk, J. Javier Ruiz-Pernía, W. M. Dawson, M. Roca, E. J. Loveridge, D. R. Glowacki, J. N. Harvey, A. J. Mulholland, I. Tuñón, V. Moliner, and R. K. Allemann, Unraveling the role of protein dynamics in dihydrofolate reductase catalysis, *Proc Natl Acad Sci USA* **110**, 16344 (2013).
- [54] P. Hanoian, C. T. Liu, S. Hammes-Schiffer, and S. Benkovic, Perspectives on electrostatics and conformational motions in enzyme catalysis, *Acc. Chem. Res.* **48**, 482 (2015).
- [55] E. Z. Eisenmesser, O. Millet, W. Labeikovsky, D. M. Korzhnev, M. Wolf-Watz, D. A. Bosco, J. J. Skalicky, L. E. Kay, and D. Kern, Intrinsic dynamics of an enzyme underlies catalysis, *Nature* **438**, 117 (2005).
- [56] S. Kale, G. Ulas, J. Song, G. W. Brudvig, W. Furey, and F. Jordan, Efficient coupling of catalysis and dynamics in the e1 component of escherichia coli pyruvate dehydrogenase multienzyme complex, *Proc Natl Acad Sci USA* **105**, 1158 (2008).
- [57] S. C. L. Kamerlin and A. Warshel, At the dawn of the 21st century: Is dynamics the missing link for understanding enzyme catalysis?, *Proteins* **78**, 1339 (2010).
- [58] Y. Togashi and A. S. Mikhailov, Nonlinear relaxation dynamics in elastic networks and design principles of molecular machines, *Proc Natl Acad Sci* **104**, 8697 (2007).
- [59] H. Flechsig and A. S. Mikhailov, Tracing entire operation cycles of molecular motor hepatitis c virus helicase in structurally resolved dynamical simulations, *Proc Natl Acad Sci* **107**, 20875 (2010).
- [60] D. R. Hekstra, K. I. White, M. A. Socolich, R. W. Henning, V. Šrajcar, and R. Ranganathan, Electric-field-stimulated pro-

- tein mechanics, *Nature* **540**, 400 (2016).
- [61] X. Ma, A. C. Hortelão, T. Patiño, and S. Sánchez, Enzyme catalysis to power micro/nanomachines, *ACS Nano* **10**, 9111 (2016).
- [62] S. Dutta, J.-P. Eckmann, A. Libchaber, and T. Tlusty, Green function of correlated genes in a minimal mechanical model of protein evolution, *Proc Natl Acad Sci USA* **115**, E4559 (2018).
- [63] J.-P. Eckmann, J. Rougemont, and T. Tlusty, Colloquium: Proteins: The physics of amorphous evolving matter, *Rev Mod Phys* **91**, 031001 (2019).
- [64] Y. Hosaka, S. Komura, and D. Andelman, Shear viscosity of two-state enzyme solutions, *Phys Rev E* **101**, 012610 (2020).
- [65] P. Bursac, G. Lenormand, B. Fabry, M. Oliver, D. A. Weitz, V. Viasnoff, J. P. Butler, and J. J. Fredberg, Cytoskeletal remodelling and slow dynamics in the living cell, *Nat Mater* **4**, 557 (2005).
- [66] A. Bernheim-Groswasser, N. S. Gov, S. A. Safran, and S. Tzlil, Living matter: Mesoscopic active materials, *Adv Mater* **30**, 1707028 (2018).
- [67] P. Sens, Stick-slip model for actin-driven cell protrusions, cell polarization, and crawling, *Proc Natl Acad Sci USA* **117**, 24670 (2020).
- [68] J.-B. Manneville, P. Bassereau, S. Ramaswamy, and J. Prost, Active membrane fluctuations studied by micropipet aspiration, *Phys Rev E* **64**, 021908 (2001).
- [69] M. C. Marchetti, J. F. Joanny, S. Ramaswamy, T. B. Liverpool, J. Prost, M. Rao, and R. A. Simha, Hydrodynamics of soft active matter, *Rev Mod Phys* **85**, 1143 (2013).
- [70] A. S. Mikhailov and R. Kapral, Hydrodynamic collective effects of active protein machines in solution and lipid bilayers, *Proc Natl Acad Sci* **112**, E3639 (2015).
- [71] H. Flechsig and A. S. Mikhailov, Simple mechanics of protein machines, *J R Soc Interface* **16**, 20190244 (2019).
- [72] H. Eyring, The activated complex in chemical reactions, *J Chem Phys* **3**, 107 (1935).
- [73] H. A. Kramers, Brownian motion in a field of force and the diffusion model of chemical reactions, *Physica* **7**, 284 (1940).
- [74] P. Hänggi, P. Talkner, and M. Borkovec, Reaction-rate theory: fifty years after kramers, *Rev Mod Phys* **62**, 251 (1990).
- [75] L. Gammaitoni, P. Hänggi, P. Jung, and F. Marchesoni, Stochastic resonance, *Rev Mod Phys* **70**, 223 (1998).
- [76] E. Pollak and P. Talkner, Reaction rate theory: What it was, where is it today, and where is it going?, *Chaos: An Interdisciplinary Journal of Nonlinear Science* **15**, 026116 (2005).
- [77] M. T. Woodside, P. C. Anthony, W. M. Behnke-Parks, K. Larizadeh, D. Herschlag, and S. M. Block, Direct measurement of the full, sequence-dependent folding landscape of a nucleic acid, *Science* **314**, 1001 (2006).
- [78] W. J. Greenleaf, K. L. Frieda, D. A. N. Foster, M. T. Woodside, and S. M. Block, Direct observation of hierarchical folding in single riboswitch aptamers, *Science* **319**, 630 (2008).
- [79] M. T. Woodside, C. García-García, and S. M. Block, Folding and unfolding single rna molecules under tension, *Curr Opin Chem Biol* **12**, 640 (2008), biopolymers/Model Systems.
- [80] K. Neupane, D. B. Ritchie, H. Yu, D. A. N. Foster, F. Wang, and M. T. Woodside, Transition path times for nucleic acid folding determined from energy-landscape analysis of single-molecule trajectories, *Phys Rev Lett* **109**, 068102 (2012).
- [81] H. Vandebroek and C. Vanderzande, The effect of active fluctuations on the dynamics of particles, motors and dna-hairpins, *Soft Matter* **13**, 2181 (2017).
- [82] C. Pozrikidis, *Boundary integral and singularity methods for linearized viscous flow* (Cambridge university press, 1992).
- [83] H. Diamant, Long-range hydrodynamic response of particulate liquids and liquid-laden solids, *Isr J Chem* **47**, 225 (2007).
- [84] R. Milo and R. Phillips, *Cell Biology by the Numbers* (CRC Press, 2015).
- [85] É. Fodor, M. Guo, N. S. Gov, P. Visco, D. A. Weitz, and F. van Wijland, Activity-driven fluctuations in living cells, *Europhys Lett* **110**, 48005 (2015).
- [86] A. Sharma, R. Wittmann, and J. M. Brader, Escape rate of active particles in the effective equilibrium approach, *Phys Rev E* **95**, 012115 (2017).
- [87] L. Caprini, U. Marini Bettolo Marconi, A. Puglisi, and A. Vulpiani, Active escape dynamics: The effect of persistence on barrier crossing, *J Chem Phys* **150**, 024902 (2019).
- [88] Y. Fily, Self-propelled particle in a nonconvex external potential: Persistent limit in one dimension, *J Chem Phys* **150**, 174906 (2019).
- [89] T. F. F. Farage, P. Krinninger, and J. M. Brader, Effective interactions in active brownian suspensions, *Phys Rev E* **91**, 042310 (2015).
- [90] U. M. B. Marconi, C. Maggi, and A. Sarracino, Active fluids within the unified coloured noise approximation, in *Flowing Matter*, edited by F. Toschi and M. Sega (Springer International Publishing, Cham, 2019) pp. 239–269.
- [91] E. Woillez, Y. Zhao, Y. Kafri, V. Lecomte, and J. Tailleur, Activated escape of a self-propelled particle from a metastable state, *Phys Rev Lett* **122**, 258001 (2019).
- [92] E. Woillez, Y. Kafri, and V. Lecomte, Nonlocal stationary probability distributions and escape rates for an active ornstein–uhlenbeck particle, *J Stat Mech Theory Exp* **2020**, 063204 (2020).
- [93] E. Woillez, Y. Kafri, and N. S. Gov, Active trap model, *Phys Rev Lett* **124**, 118002 (2020).
- [94] G. I. Bell, Models for the specific adhesion of cells to cells, *Science* **200**, 618 (1978).
- [95] S. Liu, Chapter 8 - enzymes, in *Bioprocess Engineering*, edited by S. Liu (Elsevier, Amsterdam, 2013) pp. 323 – 390.
- [96] K. Shiroguchi, H. F. Chin, D. E. Hannemann, E. Muneyuki, E. M. De La Cruz, and K. Kinoshita, Jr., Direct observation of the myosin va recovery stroke that contributes to unidirectional stepping along actin, *PLOS Biology* **9**, 1 (2011).
- [97] A. Lewalle, W. Steffen, O. Stevenson, Z. Ouyang, and J. Sleep, Single-molecule measurement of the stiffness of the rigor myosin head, *Biophysical Journal* **94**, 2160 (2008).
- [98] A. Alemany, B. Rey-Serra, S. Frutos, C. Cecconi, and F. Ritort, Mechanical folding and unfolding of protein barnase at the single-molecule level, *Biophysical Journal* **110**, 63 (2016).
- [99] Y. Hosaka, S. Komura, and A. S. Mikhailov, Mechanochemical enzymes and protein machines as hydrodynamic force dipoles: the active dimer model, *Soft Matter* **16**, 10734 (2020).
- [100] A. A. Rauscher, Z. Simon, G. J. Szöllösi, L. Gráf, I. Derényi, and A. Malnasi-Csizmadia, Temperature dependence of internal friction in enzyme reactions, *The FASEB Journal* **25**, 2804 (2011).
- [101] A. Rauscher, I. Derényi, L. Gráf, and A. Malnasi-Csizmadia, Internal friction in enzyme reactions, *IUBMB Life* **65**, 35 (2013).
- [102] J. Happel and H. Brenner, *Low Reynolds number hydrodynamics: with special applications to particulate media*, Mechanics of Fluids and Transport Processes (Springer Netherlands, 1983).
- [103] R. Mannella, Integration of stochastic differential equations on a computer, *Int J Modern Phys C* **13**, 1177 (2002).